Band-gap engineering of functional perovskites through quantum confinement and tunneling

Castelli, Ivano Eligio; Pandey, Mohnish; Thygesen, Kristian Sommer; Jacobsen, Karsten Wedel

Published in:
Physical Review B

Link to article, DOI:
10.1103/PhysRevB.91.165309

Publication date:
2015

Document Version
Publisher's PDF, also known as Version of record

Band-gap engineering of functional perovskites through quantum confinement and tunneling

Ivano E. Castelli,* Mohnish Pandey, Kristian S. Thygesen, and Karsten W. Jacobsen
Center for Atomic-scale Materials Design, Department of Physics, Technical University of Denmark, DK-2800 Kongens Lyngby, Denmark
(Received 30 December 2014; revised manuscript received 25 March 2015; published 24 April 2015)

An optimal band gap that allows for a high solar-to-fuel energy conversion efficiency is one of the key factors to achieve sustainability. We investigate computationally the band gaps and optical spectra of functional perovskites composed of layers of the two cubic perovskite semiconductors $BaSnO_3$ and $BaTaO_2N$. Starting from an indirect gap of around 3.3 eV for $BaSnO_3$ and a direct gap of 1.8 eV for $BaTaO_2N$, different layerings can be used to design a direct gap of the functional perovskite between 2.3 and 1.2 eV. The variations of the band gap can be understood in terms of quantum confinement and tunneling. We also calculate the light absorption of the different heterostructures and demonstrate a large sensitivity to the detailed layering.

DOI: 10.1103/PhysRevB.91.165309 PACS number(s): 68.35.bg, 73.21.Ac, 73.20.−r, 78.20.−e

I. INTRODUCTION

Functional oxides form a fascinating class of materials exhibiting a large range of phenomena and with great potential for technological applications. Some of their properties include high-temperature superconductivity, multiferroic and half-metallic behavior, thermoelectric, magnetocaloric, and photoconductivity effects, transport phenomena, and catalytic properties [1]. The oxides in the perovskite structure constitute an interesting subclass with high stability and new underexplored possibilities for producing layered heterostructures with atomically well-defined interfaces. Effects of quantum confinement in atomically layered perovskites have been discussed in several different heterosystems [2]. Yoshimatsu *et al.* [3–5] have studied quantum wells of the metal $SrVO_3$ embedded in an insulator, $SrTiO_3$, with photoemission, demonstrating that modifications of the electronic structure develop below six layers of $SrVO_3$ and that for a single layer a substantial gap appears. Other studies include confinement effects on the magnetic structure of $LaMnO_3/SrMnO_3$ superlattices [6] and recent investigations of how non-Fermi-liquid behavior appears when a $SrTiO_3$ quantum well embedded in $SmTiO_3$ is sufficiently thin [7]. More recently, Grote *et al.* [8] have investigated how to tune the band gap of tin- and lead-halide perovskites through effects of atomic layering and quantum confinement.

In the present work, we investigate the band gaps and the light-absorption properties of functional perovskites obtained by stacking cubic perovskite planes, with general formula ABO_3, in one direction (say, the z axis) while the other two directions preserve the cubic symmetry, as shown in Fig. 1. The possibilities for producing such structures are numerous, but little is known about the potential for systematic, quantitative control of their properties. We show that a large variation of the band gap can be obtained and that the size of the band gap for a particular stacking sequence can be understood in terms of confinement and tunneling behavior. Using these ingredients, an engineering of the band gap can be pursued to tune the gap to a desired window. This approach could potentially be used to achieve high efficiencies in light-harvesting devices.

More specifically, we consider combinations of the two cubic perovskite semiconductors $BaSnO_3$ and $BaTaO_2N$, indicated with α and β in Fig. 1, respectively [9]. The choice of these two materials as building blocks is based on the fact that both $BaSnO_3$ and $BaTaO_2N$ have been previously selected as good materials for light harvesting and photocatalytic water splitting [10,11] and their crystal lattices are rather similar, with the consequence that the obtained layered structure [12] will not be subjected to high stress.

All of the calculations presented in this work are performed in the framework of density functional theory (DFT) using the electronic structure code GPAW [13,14]. Due to the well-known problem of standard DFT with the underestimation of the band gaps, the gaps have been calculated using the GLLB-SC potential by Gritsenko, van Leeuwen, van Lenthe, and Baerends (GLLB) [15], modified by Kuisma *et al.* [16] to include the correlation for solids (-SC). This potential has been shown to provide realistic estimates of band gaps when compared with other more advanced computational methods and experiments for a range of semiconductors and insulators including oxides without too strong correlation effects [10,17–19]. One reason for the favorable comparison is the addition to the DFT Kohn-Sham gap of the so-called derivative discontinuity, which is explicitly calculated in the GLLB-SC approach. We have furthermore performed hybrid calculations using the functional proposed by Heyd, Scuseria, and Ernzerhof (HSE06) [20,21] as a comparison for a subset of the layered materials investigated in this work.

II. BAND GAPS

The compounds that we study here are all obtained by stacking n_α layers of α with n_β layers of β, where $1 \leqslant n_{\alpha(\beta)} \leqslant 6$, and then repeating this unit periodically. The lattice parameter is taken equal to the average value of the lattices of α and β (4.1 Å [22]). $BaSnO_3$ and $BaTaO_2N$ have been frozen in their perfect cubic perovskite symmetry, i.e., without any distortion. Even though distortions usually have large effects on the band gaps, $BaSnO_3$ and $BaTaO_2N$ have a high cubicity so that the changes in the band gaps are expected to be small. Keeping the structures frozen in the cubic symmetry furthermore allows us to analyze the changes in the electronic

*ivca@fysik.dtu.dk. Present address: Theory and Simulation of Materials (THEOS) and National Center for Computational Design and Discovery of Novel Materials (MARVEL), École Polytechnique Fédérale de Lausanne, CH-1015 Lausanne, Switzerland.

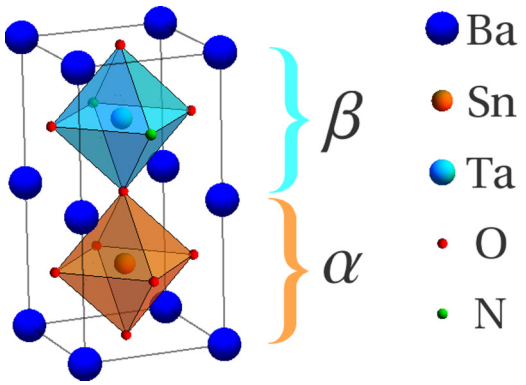

FIG. 1. (Color online) Unit cell of the $\alpha\beta$ structure. The cubic perovskite planes are stacked in the z direction, while the x and y directions maintain the usual periodicity of a cubic perovskite. α indicates the $BaSnO_3$ perovskite, and β the $BaTaO_2N$.

properties of the materials due only to the different stackings, regardless of any changes caused by structure relaxation.

Using GLLB-SC, $BaSnO_3$ shows an indirect band gap between the Γ and R points of 3.33 eV, while $BaTaO_2N$ is found to have a direct band gap at Γ of 1.84 eV. This compares favorably with experiments where the optical gaps have been measured, through diffuse reflectance spectra, to 3.1 and 1.9 eV for $BaSnO_3$ [23] and $BaTaO_2N$ [24], respectively. HSE calculations slightly underestimate the gaps (2.89 eV for $BaSnO_3$ and 1.71 eV for $BaTaO_2N$).

Figure 2 reports the band gaps for the 36 $\alpha_{n_\alpha}\beta_{n_\beta}$ structures as a function of the number of α and β planes. The gaps vary considerably spanning a region of 1 eV, illustrating the high degree of tunability of the band gap. The simplest combination with only one layer of α and β in the heterostructure gives the widest gap with a value of 2.26 eV, not too far from the average of the band gaps of the two constituent cubic perovskites. (For comparison, the HSE method gives again a slightly lower value of 2.04 eV.) More complex combinations exhibit reduced band

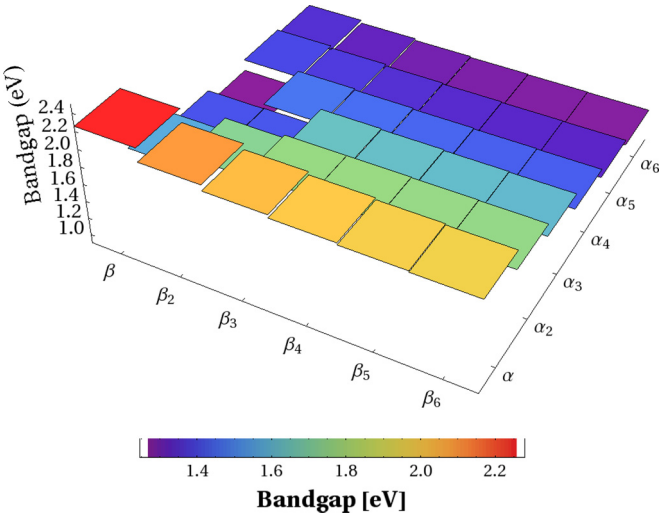

FIG. 2. (Color online) Calculated band gaps as a function of the number of α ($BaSnO_3$) and β ($BaTaO_2N$) layers. Each rectangle in the plot represents a layered periodic structure with sequence $\alpha_n\beta_m$.

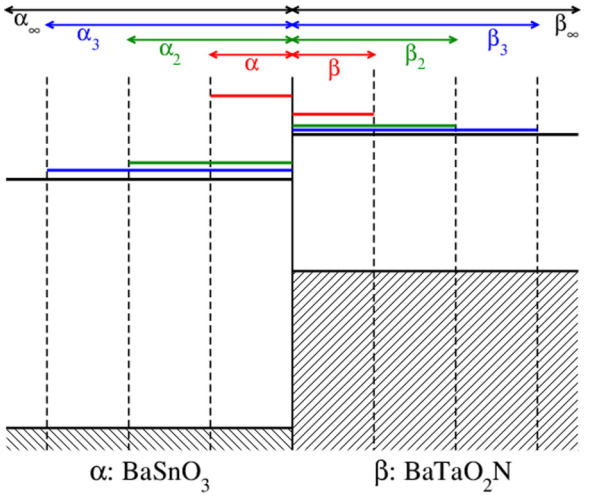

FIG. 3. (Color online) Sketch of the electronic level positions at an interface between layers of $BaSnO_3$ and $BaTaO_2N$. When the layer thickness is reduced, the local position of the conduction-band edge moves up due to confinement.

gaps depending on their composition. As we shall show in the following, the significant complicated variation of the band gap shown in Fig. 2 can essentially be understood in terms of electronic confinement and tunneling effects.

In Fig. 3, we sketch how the local band edges are positioned relative to each other for different layer thicknesses. For the thickest layer structure, $\alpha_6\beta_6$, we have the smallest band gap of 1.26 eV. The state at the valence-band maximum (VBM) is composed mainly of N_{2p} orbitals with a minor contribution from the O_{2p} orbitals and is located in the β part of the material. In fact, all of the mixed compositions have a direct band gap at the Γ point, with the VBM state of this character located in the β part of the material. The character of the VBM state can, for example, be seen in Figs. 4(a) and 4(c) for the $\alpha\beta$ and $\alpha_2\beta$ structures, respectively. Not only is the character of the VBM state the same for all structures, but the calculations also indicate that it does not move much relative to a low-lying atomic state in $BaTaO_2N$, and we shall therefore regard this level as fixed in the following and ascribe the variations to changes in the conduction band.

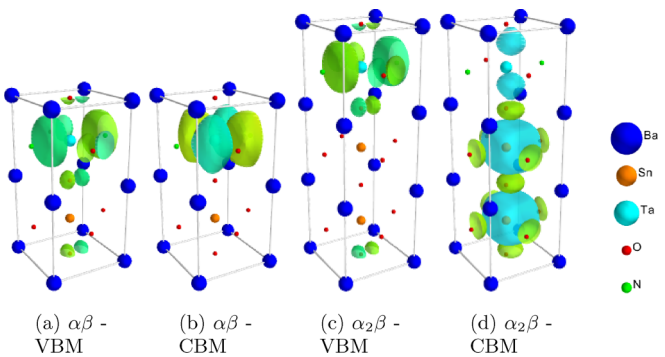

FIG. 4. (Color online) Wave functions of states at the valence-band maximum (VBM) and the conduction-band minimum (CBM) for some combinations of α and β layers.

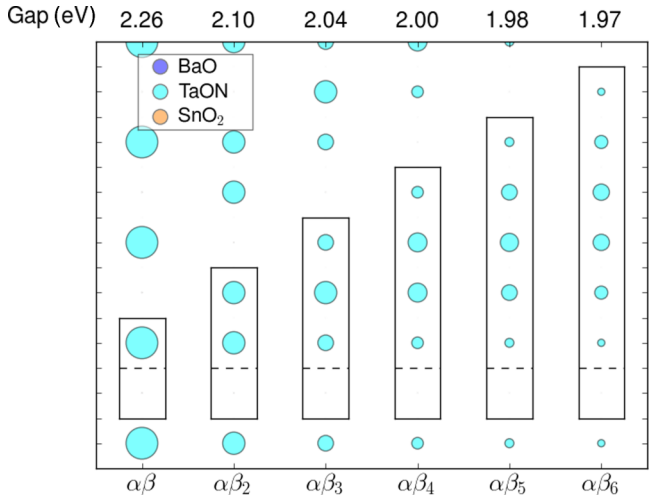

FIG. 5. (Color online) The figure illustrates the weights of the CBM state in real space. The vertical axes are along the stacking direction of the material and the areas of the circles indicate the weights of the CBM state for a particular atomic xy plane. The boxes show the extent of the supercell in the direction of the stacking (z), and the dashed lines mark the interfaces between the α and β layers. Above the figure, the calculated band gaps for the different stacking sequences are denoted. The CBM state is mainly composed of Ta d orbitals, as shown in Fig. 4(b).

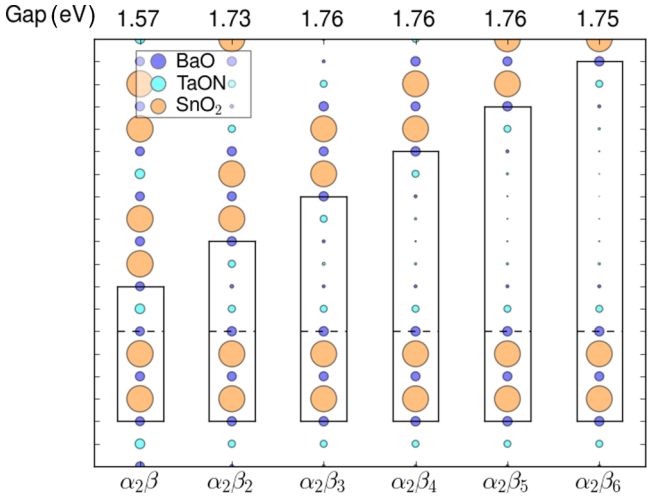

FIG. 6. (Color online) Weight of the CBM state in each xy plane of the $n_\alpha = 2$ structure. The CBM state is now composed of Sn s states, with some tunneling through the TaON plane [Fig. 4(d)]. The tunneling progressively reduces with the increase of β layers.

To understand the variation of the conduction-band minimum in Fig. 3, we first consider the compounds with the formula $\alpha\beta_{n_\beta}$, where the band gap decreases as a function of the number of β layers. The CBM states for these systems are located only on the TaON plane, as shown in Fig. 5, and generated by the Ta_{5d} orbitals, as plotted in Fig. 4(b) for the $\alpha\beta$ case. The variation of the band gap as a function of n_β is a result of quantum confinement. The empty states in the single α layer are shifted up out of reach, and the CBM state in β becomes less confined with the increase of the number of β layers in the $\alpha\beta_{n_\beta}$ structures, as can be seen in Fig. 5. The reduction of the confinement results in a down-shift of the CBM level and thus a reduced band gap, as also sketched in Fig. 3.

The situation is radically different for all the combinations $\alpha_{n_\alpha}\beta_{n_\beta}$, with $n_\alpha \geqslant 2$. Now the CBM state is not located in β, but in α. It is located mainly on the Sn_{5s} orbitals, as shown in Fig. 4(d). If, for example, we consider the compounds $\alpha_2\beta_n$, the CBM state is localized in the α_2 layers and essentially looks the same, as seen in Fig. 6. The band gap is therefore also largely unchanged for $n \geqslant 3$. For $n = 2$, a small reduction relative to the situation with $n \geqslant 3$ is seen and this reduction becomes even larger for $n = 1$ (see Fig. 2). We ascribe this reduction to quantum tunneling through the thin β layers. As can be seen in Fig. 6, the CBM states decay into the β layers and the tunneling coupling, for small thicknesses, will result in a lowering of the CBM level and thus a decrease of the band gap.

The interplay between quantum confinement and tunneling is seen most clearly for the $n_\beta = 1$ systems (Fig. 7). Ignoring the $\alpha\beta$ structure that has a different nature for the CBM level with respect to the other systems, the CBM state becomes less confined with the increase of the number of α layers, with the consequence of a decrease in the band gap. And as we have seen, the band gap is further reduced because of tunneling through the single β TaON layer. However, for larger thicknesses of the α layer, the tunneling effect is reduced because the now less-confined CBM state has lower amplitude at the interface. This interplay between confinement and tunneling leads to the increase of the band gap between $n_\alpha = 4$ and $n_\alpha = 5$.

As we have seen, the variation of the band gaps for the different periodic $\alpha_n\beta_m$ compounds can be understood from the confinement effects shown in the level diagram in Fig. 3 together with additional tunneling effects if β_1 or β_2 layers are present. Does this lesson apply to more complicated sequences

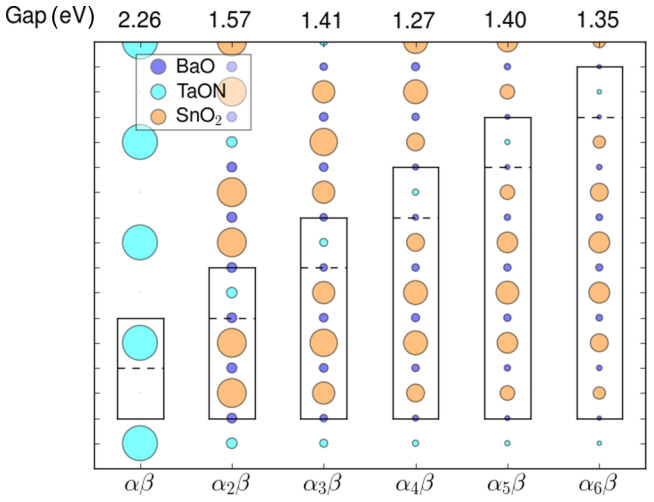

FIG. 7. (Color online) Weight of the CBM state in each xy plane of the $n_\beta = 1$ structure. The character of the CBM state changes drastically with n_α: TaON is responsible for the CBM state for the $n_\alpha = 1$ structure, while for $n_\alpha > 1$, it is SnO_2 [Figs. 4(b) and 4(d)]. The tunneling across the TaON plane has an effect until $n_\alpha = 4$.

of layers? Some test calculations seem to indicate so. A compound with the periodic repetition of $\alpha\beta\alpha\beta_{n_\beta}$ reproduces exactly the same gaps as the $\alpha\beta_{n_\beta}$. This is to be expected since from the level diagram in Fig. 3 we should expect the CBM state to be located in the β_{n_β} layer with little tunneling through the α layers. Another example is the systems with sequence $\alpha\beta\alpha_{n_\alpha}\beta$, which exhibit a small increase (up to about 0.2 eV) of the band gap for $n_\alpha \geqslant 2$ as compared to the $\alpha_{n_\alpha}\beta$ compounds. This can be understood in terms of reduced tunneling because the α_{n_α} layers are now separated by $\beta\alpha\beta$ instead of a single β layer reducing the tunneling effect.

III. OPTICAL PROPERTIES

A number of technological applications such as photovoltaics or photocatalysis depend on the availability of efficient absorbers of light in the visible spectrum. This requires an appropriate band gap of the material, and band-gap tuning is therefore a key issue. However, the band gap does not by itself provide any information about the magnitude of the matrix elements responsible for light absorption. For symmetry reasons, the light absorption can be dipole allowed or forbidden and—in particular for heterostructures—the transitions may take place between states with different degree of spatial overlap, giving rise to large variations of the absorption strengths.

To address this issue, we perform linear response calculations [25], using the adiabatic local density approximation (ALDA), and determine the optical absorption of the investigated systems focusing for simplicity on the systems with $n_\alpha = 1$ or $n_\beta = 1$ [26]. The optical absorption spectrum is calculated using time-dependent density functional theory (TDDFT) from the density response function χ. The response function evaluated at point $\mathbf{r}$ to first order in a time-dependent perturbation of frequency ω applied at point $\mathbf{r}'$ is $\chi(\mathbf{r},\mathbf{r}',\omega) = \delta n(\mathbf{r},\omega)/\delta V_{\text{ext}}(\mathbf{r}',\omega)$, where δn is the induced density under the perturbation caused by the external potential V_{ext}.

The microscopic dielectric matrix is defined as

$$\epsilon^{-1}_{\mathbf{G}\mathbf{G}'}(\mathbf{q},\omega) = \delta_{\mathbf{G}\mathbf{G}'} + \frac{4\pi}{|\mathbf{q}+\mathbf{G}|^2}\chi_{\mathbf{G}\mathbf{G}'}(\mathbf{q},\omega), \qquad (1)$$

where $\mathbf{G}$ and $\mathbf{G}'$ are reciprocal lattice vectors, and $\mathbf{q}$ is a wave vector of the first Brillouin zone. The optical absorption spectrum is given by $\text{Im}\epsilon(\mathbf{q}\to 0,\omega)$, where $\epsilon(\mathbf{q}\to 0,\omega) = \frac{1}{\epsilon^{-1}_{\mathbf{00}}(\mathbf{q}\to 0,\omega)}$.

Figure 8 shows the optical absorption for the $n_\alpha = 1$ systems. In the plot, we distinguish between the case where the light is polarized along the xy and the z directions. The xy plane, in fact, maintains the cubic symmetry, while the stacking of the layers takes place in the z direction. For these compounds, the CBM and VBM states are located in the same region of space, namely, in the TaON layers, and thus the absorption starts at the direct band gap and is quite intense, especially for polarizations in the xy direction. The situation is different for the $n_\beta = 1$ systems (Fig. 9), where the VBM state is located in the TaON layer, while the CBM state has most weight on the BaO_2 layers. The absorption here starts at much higher energies than the band gap (except for the $\alpha\beta$ compound, in black in the figure, which has the VBM and

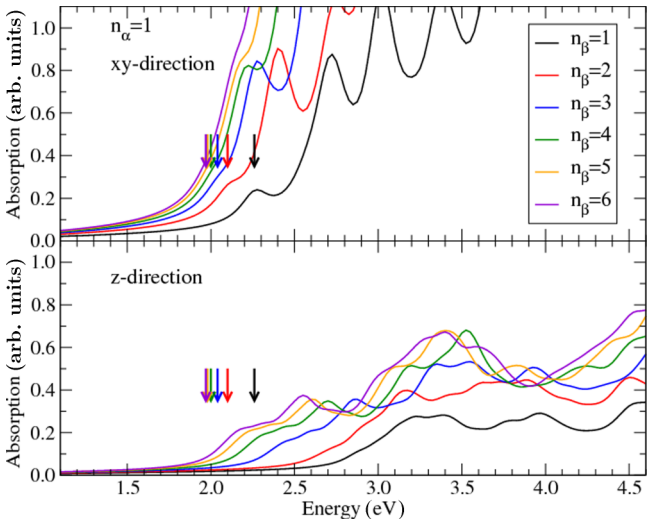

FIG. 8. (Color online) Calculated optical absorption for the $n_\alpha = 1$ systems. The direct band gaps are indicated with vertical arrows.

CBM states located in the same region). The first transition with appreciable weight is between two TaON states in the β layer, and the absorption curves are therefore fairly similar, independent of the band gap.

Table I reports the efficiencies of the two sequences. The efficiency is calculated as the percentage of the collected photons of the global solar spectrum at AM1.5 [27]. As also shown in Figs. 8 and 9, the efficiency is higher for light polarized in the xy direction than along z. $\alpha\beta_2$ and $\alpha_2\beta$ are almost comparable because the higher absorption properties of the former are balanced by the lower band gap of the latter, and the two systems collect almost the same amount of photons. The efficiency of the $\alpha\beta_{n_\beta}$ sequence always increases with the number of layers, while the one of $\alpha_{n_\alpha\beta}$ decreases even though the gap closes.

The calculations thus indicate that the absorption cross section at the $\alpha - \beta$ interface is quite limited and that the

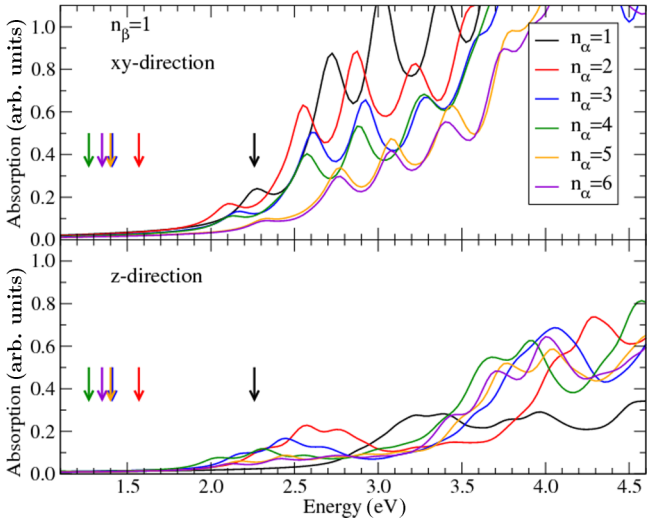

FIG. 9. (Color online) Calculated optical absorption for the $n_\beta = 1$ systems. The direct band gaps are indicated with vertical arrows.

TABLE I. Gap (in eV) and photon-absorption efficiency η (in %, for light polarized in the xy and z directions) of the sequences $\alpha\beta_{n_\beta}$ and $\alpha_{n_\alpha}\beta$, calculated for a thickness of 10^{-7} m. The efficiency calculated for the pure α and β cubic perovskites is included for comparison.

	Gap	η^{xy}	η^{z}		Gap	η^{xy}	η^{z}
α	3.33	0.1	0.1	β	1.84	14.9	6.4
$\alpha\beta$	2.26	4.3	0.9	$\alpha\beta$	2.26	4.3	0.9
$\alpha\beta_2$	2.10	7.0	1.5	$\alpha_2\beta$	1.57	5.3	2.1
$\alpha\beta_3$	2.04	8.9	2.4	$\alpha_3\beta$	1.41	4.3	2.0
$\alpha\beta_4$	2.00	10.0	3.0	$\alpha_4\beta$	1.27	4.1	2.0
$\alpha\beta_5$	1.98	10.7	3.5	$\alpha_5\beta$	1.40	2.8	1.5
$\alpha\beta_6$	1.97	11.3	3.8	$\alpha_6\beta$	1.35	2.6	1.5

band-edge states have to be localized in the same layers to obtain efficient absorption.

IV. CONCLUSIONS

In this work, we have investigated the electronic properties of perovskite heterostructures obtained by stacking $BaSnO_3$ and $BaTaO_2N$ layers. The band gap is seen to be tunable over the wide range of around 1 eV and the variation can be understood in terms of quantum confinement and tunneling. Confinement leads to up-shifts of the conduction-band minimum and thus to increase of the band gap, while tunneling effects reduce the confinement and lead to lower band gap. The tunneling effects are seen to decay over a few perovskite unit cells. The systems studied here are close to cubic and with similar lattice constants, but in general band-gap formation in layered perovskites can be expected to depend sensitively also on strain and lattice distortions/reconstructions [28].

The calculated optical absorption spectra for the heterostructures indicate that high absorption is only obtained if the VBM and CBM states are localized in the same spatial region. The design of heterostructures for efficient visible-light absorption therefore requires not only appropriate band gaps, but also tailored band-edge states with proper spatial overlap.

The stacking of $BaSnO_3$ and $BaTaO_2N$ layers that we have described here is a type-II heterojunction with the conduction band of $BaSnO_3$ above the valence band of $BaTaO_2N$. A type-I heterojunction can be designed using different perovskites. One example is $LaAlO_3$ (as α) and $LaTiO_2N$ (as β), with a calculated indirect band gap between Γ and R points of 6.11 and a direct gap at the Γ point of 1.49 eV, respectively, and where the band edges of $LaTiO_2N$ are placed in between the edges of $LaAlO_3$. Preliminary results show that due to the large band gap of α, there is no tunneling through the α layer and there is already a full confinement of the β layers with a single α [29]. In addition, the band gaps of the layered combinations are direct, with the VBM formed by N_{2p} orbitals and the CBM composed of Ti_{3d}. Also in this case, the stacking has the effect of placing the VBM and CBM closer together spatially. This fact might increase the absorption properties of the materials and, together with the possibility of tuning the band gap using quantum confinement and tunneling, can be used to design novel light-harvesting heterojunctions.

ACKNOWLEDGMENTS

The authors acknowledge support from the Catalysis for Sustainable Energy (CASE) initiative funded by the Danish Ministry of Science, Technology and Innovation, and from the Center on Nanostructuring for the Efficient Energy Conversion (CNEEC) at Stanford University, an Energy Frontier Research Center founded by the U.S. Department of Energy, Office of Science, Office of Basic Energy Sciences under Award No. DE-SC0001060. K.S.T. acknowledges support from the Danish Council for Independent Research Sapere Aude Program through Grant No. 11-1051390. The Center for Nanostructured Graphene is sponsored by the Danish National Research Foundation, Project No. DNRF58.

[1] F. M. Granozio, G. Koster, and G. Rijnders, Mater. Res. Bull. **38**, 1017 (2013).
[2] S. Stemmer and A. J. Millis, Mater. Res. Bull. **38**, 1032 (2013).
[3] K. Yoshimatsu, T. Okabe, H. Kumigashira, S. Okamoto, S. Aizaki, A. Fujimori, and M. Oshima, Phys. Rev. Lett. **104**, 147601 (2010).
[4] K. Yoshimatsu, E. Sakai, M. Kobayashi, K. Horiba, T. Yoshida, A. Fujimori, M. Oshima, and H. Kumigashira, Phys. Rev. B **88**, 115308 (2013).
[5] K. Yoshimatsu, K. Horiba, H. Kumigashira, T. Yoshida, A. Fujimori, and M. Oshima, Science **333**, 319 (2011).
[6] T. S. Santos, B. J. Kirby, S. Kumar, S. J. May, J. A. Borchers, B. B. Maranville, J. Zarestky, S. G. E. te Velthuis, J. van den Brink, and A. Bhattacharya, Phys. Rev. Lett. **107**, 167202 (2011).
[7] C. A. Jackson, J. Y. Zhang, C. R. Freeze, and S. Stemmer, Nat. Commun. **5**, 1 (2014).
[8] C. Grote, B. Ehrlich, and R. F. Berger, Phys. Rev. B **90**, 205202 (2014).
[9] We consider, for simplicity, only the simplest ordered structure of the nitrogen atoms. Some check calculations within the unit cells we use indicate that exchanging O and N atoms so that the number of O and N neighbors of the Ta atoms stays fixed only gives minor changes to both the stability and the band gap (changes less than 0.1 eV). If the O and N coordination of the Ta atoms is changed, the stability is significantly decreased.
[10] I. E. Castelli, T. Olsen, S. Datta, D. D. Landis, S. Dahl, K. S. Thygesen, and K. W. Jacobsen, Energy Environ. Sci. **5**, 5814 (2012).
[11] I. E. Castelli, D. D. Landis, K. S. Thygesen, S. Dahl, I. Chorkendorff, T. F. Jaramillo, and K. W. Jacobsen, Energy Environ. Sci. **5**, 9034 (2012).
[12] Layered perovskite usually is the name given to ABO_3 perovskites separated by some motifs. Some examples are the Ruddlesden-Popper and the Dion-Jacobson phases. In this work,

with layered perovskite, we indicate layers of cubic perovskites stacked in the z direction.

[13] J. J. Mortensen, L. B. Hansen, and K. W. Jacobsen, Phys. Rev. B **71**, 035109 (2005).

[14] J. Enkovaara, C. Rostgaard, J. J. Mortensen, J. Chen, M. Dulak, L. Ferrighi, J. Gavnholt, C. Glinsvad, V. Haikola, H. A. Hansen, H. H. Kristoffersen, M. Kuisma, A. H. Larsen, L. Lehtovaara, M. Ljungberg, O. Lopez-Acevedo, P. G. Moses, J. Ojanen, T. Olsen, V. Petzold, N. A. Romero, J. Stausholm-Møller, M. Strange, G. A. Tritsaris, M. Vanin, M. Walter, B. Hammer, H. Hakkinen, G. K. H. Madsen, R. M. Nieminen, J. K. Nørskov, M. Puska, T. T. Rantala, J. Schiøtz, K. S. Thygesen, and K. W. Jacobsen, J. Phys. Condens. Matter **22**, 253202 (2010).

[15] O. Gritsenko, R. van Leeuwen, E. van Lenthe, and E. J. Baerends, Phys. Rev. A **51**, 1944 (1995).

[16] M. Kuisma, J. Ojanen, J. Enkovaara, and T. T. Rantala, Phys. Rev. B **82**, 115106 (2010).

[17] F. Hüser, T. Olsen, and K. S. Thygesen, Phys. Rev. B **87**, 235132 (2013).

[18] I. E. Castelli, J. M. García-Lastra, F. Hüser, K. S. Thygesen, and K. W. Jacobsen, New J. Phys. **15**, 105026 (2013).

[19] I. E. Castelli, F. Hüser, M. Pandey, H. Li, K. S. Thygesen, B. Seger, A. Jain, K. A. Persson, G. Ceder, and K. W. Jacobsen, Adv. Energy Mater. **5**, 1400915 (2015).

[20] J. Heyd, G. E. Scuseria, and M. Ernzerhof, J. Chem. Phys. **118**, 8207 (2003).

[21] A. V. Krukau, O. A. Vydrov, A. F. Izmaylov, and G. E. Scuseria, J. Chem. Phys. **125**, 224106 (2006).

[22] The lattice parameters of α and β calculated with the PBEsol functional [30] are 4.12 and 4.08 Å, respectively, in very good agreement with the experimental values (4.11 Å for both α [31] and β [32]).

[23] H. Mizoguchi, H. W. Eng, and P. M. Woodward, Inorg. Chem. **43**, 1667 (2004).

[24] D. Yamasita, T. Takata, M. Hara, J. N. Kondo, and K. Domen, Solid State Ionics **172**, 591 (2004).

[25] J. Yan, J. J. Mortensen, K. W. Jacobsen, and K. S. Thygesen, Phys. Rev. B **83**, 245122 (2011).

[26] TDDFT-ALDA does not include excitonic effects. However, the exciton binding energy E_{exc} can be estimated using the Wannier-Mott model,

$$E_{\mathrm{exc}} = R\frac{\mu}{m}\frac{1}{\epsilon_{\mathrm{M}}^2},$$

where $R = 13.606$ eV, $\frac{1}{\mu} = \frac{1}{\mu_{\mathrm{c}}^*} + \frac{1}{\mu_{\mathrm{v}}^*}$, with μ_{c}^* and μ_{v}^* the hole and electron effective masses at the CBM and VBM, respectively, and ϵ_{M} is the macroscopic dielectric constant. Based on this, we estimate the exciton binding energies for $BaSnO_3$ and $BaTaO_2N$ to be of the order of 0.3 and 0.1 eV, respectively, and about 0.2 eV for the $\alpha\beta$ sequence.

[27] The efficiency η is given by

$$\eta = \frac{1}{n_{\mathrm{tot}}}\int_{\mathrm{gap}}^{\infty} ph_{\mathrm{abs}}(E)n_{\mathrm{ph}}(E)dE,$$

where n_{tot} is the total number of photons from the sun measured at AM1.5, $ph_{\mathrm{abs}}(E)$ is the photon absorptivity of the material, and $n_{\mathrm{ph}}(E)$ is the number of sun photons as a function of energy E, in eV. The photon absorptivity depends on the the absorption coefficient $\alpha(E)$ and on the depth of the material along the absorption direction L: $ph_{\mathrm{abs}}(E) = 1 - e^{-\alpha(E)L}$. The absorption coefficient is $\alpha(E) = \frac{2Ek(E)}{\hbar c}$, where $\hbar$ and c are the Planck constant and the speed of light, respectively, and k is obtained from the absorption spectrum as $k^2 = \frac{1}{2}(-\mathrm{Re}\epsilon + \sqrt{\mathrm{Re}^2\epsilon + \mathrm{Im}^2\epsilon})$.

[28] H. Li, I. E. Castelli, K. S. Thygesen, and K. W. Jacobsen, Phys. Rev. B **91**, 045204 (2015).

[29] The calculated gaps for this combination, as well as for the $BaSnO_3$-$BaTaO_2N$, are available in the Computational Materials Repository at https://cmr.fysik.dtu.dk/.

[30] J. P. Perdew, A. Ruzsinszky, G. I. Csonka, O. A. Vydrov, G. E. Scuseria, L. A. Constantin, X. Zhou, and K. Burke, Phys. Rev. Lett. **100**, 136406 (2008).

[31] H. Mizoguchi, P. M. Woodward, C.-H. Park, and D. A. Keszler, J. Am. Chem. Soc. **126**, 9796 (2004).

[32] F. Pors, R. Marchand, Y. Laurent, P. Bacher, and G. Roult, Mater. Res. Bull. **23**, 1447 (1988).